Journal Pre-proof

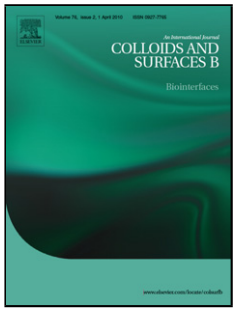

Bacterioruberin from Haloarchaea plus dexamethasone in ultra-small macrophage-targeted nanoparticles as potential intestinal repairing agent

Leticia Herminia Higa, Priscila Schilrreff, Andrés Martín Briski, Horacio Emanuel Jerez, Marcelo Alexandre de Farias, Rodrigo Villares Portugal, Eder Lilia Romero, Maria Jose Morilla

PII: S0927-7765(20)30191-0

DOI: https://doi.org/10.1016/j.colsurfb.2020.110961

Reference: COLSUB 110961

To appear in: *Colloids and Surfaces B: Biointerfaces*

Received Date: 25 November 2019

Revised Date: 20 February 2020

Accepted Date: 9 March 2020

Please cite this article as: Higa LH, Schilrreff P, Martín Briski A, Jerez HE, de Farias MA, Villares Portugal R, Romero EL, Morilla MJ, Bacterioruberin from Haloarchaea plus dexamethasone in ultra-small macrophage-targeted nanoparticles as potential intestinal repairing agent, *Colloids and Surfaces B: Biointerfaces* (2020), doi: https://doi.org/10.1016/j.colsurfb.2020.110961

Bacterioruberin from Haloarchaea plus dexamethasone in ultra-small macrophage-targeted nanoparticles as potential intestinal repairing agent

Leticia Herminia Higa[1#], Priscila Schilrreff[1#], Andrés Martín Briski[1], Horacio Emanuel Jerez[1], Marcelo Alexandre de Farias[2], Rodrigo Villares Portugal[2], Eder Lilia Romero[1] & Maria Jose Morilla[1*]

[1] Nanomedicine Research and Development Centre, Science and Technology Department, National University of Quilmes, Roque Saenz Peña 352, Bernal, B1876BXD, Argentina.

[2] Brazilian Nanotechnology National Laboratory, CNPEM, Caixa Postal 6192, CEP 13.083-970, Campinas, São Paulo, Brazil.

# authors contributed equally to these work

* Coresponding author

Maria Jose Morilla

Nanomedicine Research & Development Center, Departamento de Ciencia y Tecnología, Universidad Nacional de Quilmes. Roque Saenz Peña 352, Bernal, B1876 BXD

Tel +541143657100

Fax +541143657132

email: jmorilla@unq.edu.ar

Statistical summary:

Total number of words: 5769

Tables: 1

Figures: 4

Supplementary figures: 4

Supplementary tables: 2

Graphical abstract

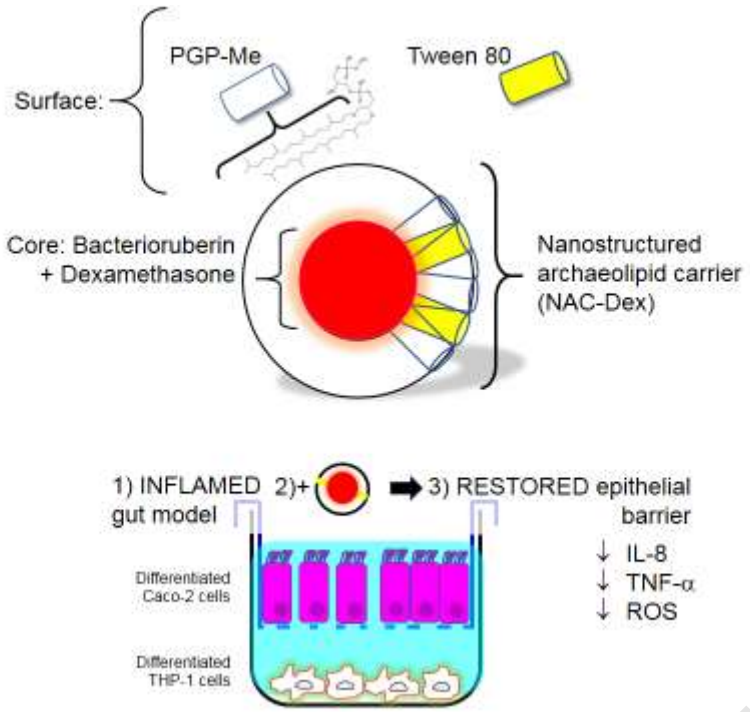

Highlights

- NAC-Dex reduced TNF-α, IL-8 and ROS on a gut inflammation model.
- NAC-Dex reversed the morphological changes induced by inflammation and increased the TEER
- NAC-Dex could be excellent candidate as intestinal barrier repairer

Abstract
Oral administration of antioxidant and anti-inflammatory drugs have the potential to improve the current therapy of inflammatory bowel disease. Success of oral treatments, however, depends on the capacity of drugs to remain structurally stable along the gastrointestinal tract, and on the feasibility of accessing the target cells. Delivering anti-inflammatory and antioxidant drugs to macrophages using targeted nanoparticles, could make treatments more efficient. In this work structural features and *in vitro* activity of macrophage-targeted nanostructured archaeolipid carriers (NAC) containing the high antioxidant dipolar C50 carotenoid bacterioruberin (BR) plus dexamethasone (Dex): NAC-Dex, are described. Ultra-small (66 nm), -32 mV ζ potential, 1200 μg Dex /ml NAC-Dex, consisted of a compritol and BR core, covered by a shell of *sn* 2,3 ether linked archaeolipids and Tween 80 (2: 2: 1.2: 3 % w/w) were obtained. NAC-Dex were extensively captured by macrophages and Caco-2 cells and displayed high anti-inflammatory and antioxidant activities on a gut inflammation model made of Caco-2 cells and lipopolysaccharide stimulated THP-1 derived macrophages reducing 65 % and 55 % TNF-α and IL-8 release, respectively and 60 % reactive oxygen species production. NAC-Dex also reversed the morphological changes induced by inflammation and increased the transepithelial electrical resistance, partly reconstituting the barrier function. Activity of BR and Dex in NAC-Dex was partially protected after simulated gastrointestinal digestion, improving the chances of BR-Dex joint activity. Results suggest that oral NAC-Dex deserve further exploration as intestinal barrier repairing agent.

Keywords: oral delivery; inflammatory bowel diseases; Caco-2/THP-1 co-culture

1. Introduction

Inflammatory bowel diseases (IBD) such as Crohn's disease and ulcerative colitis, are incurable relapsing disorders of the gastrointestinal tract (GIT). IBD are characterized by chronic inflammation and epithelial injury induced by the uncontrolled activation of the mucosal immune system [1]. The pathogenesis and progression of the inflammatory cascade are attributed to genetic, immunological, microbiome, and environmental factors [2, 3]. Oxidative stress (OS) is the a major responsible for IBD pathophysiology, rather than a consequence of chronic inflammation of the intestinal mucosa [4, 5, 6]. Enhanced production of reactive oxygen and nitrogen species (ROS and RNS, respectively) is associated with chronic intestinal inflammation in the early stages of IBD, amplification of inflammatory process, destruction of mucosa, development of fibrosis [7, 8]. Moreover, the impaired antioxidant activity in IBD patients is known to favour the progression of disease [9]. IBD patients require life-long medication and most often surgery. Treatments are mainly focused on reducing inflammation with oral sulfasalazine, corticosteroids or intravenous infliximab that blocks TNF-α [10] or by supressing the immune system with thiopurines and cyclosporine. However, the adverse effects associated with these drugs used over prolonged periods and the high relapse rate limit their use [10, 11]. Despite of the connection between OS and IBD and the fact that co-administration of anti-inflammatory drugs and antioxidants has shown clinical benefits in IBD patients [12-14], no specific antioxidant treatment against IBD is available. Success of oral treatments, however, depends on the capacity of drugs to remain structurally stable along the GI transit, and on the feasibility of accessing the target cells. Delivering anti-inflammatory and antioxidant drugs to macrophages and dendritic cells with targeted nanoparticles, could make IBD treatments more effective than conventional therapies.

Halophilic archaea produce polar (PA) and neutral archaeolipids (NA) with unique properties, different to polar lipids from Eukarya and Bacteria lipids. PA are *sn* 2,3 saturated isoprenoid chains linked via ether bonds to glycerol. Unlike liposomes prepared with phospholipids from plants or animal sources (*sn* 1,2 acyl chains linked to glycerol by ester bonds) archaeosomes (ARC) made with PA from halophilic archaebacteria *Halorubrum tebenquichense* are colloidal and chemically resistant to stress such as heat sterilization, storage under cold-free conditions [15], nebulization [16] and gastrointestinal digestion [17]. Besides, the main component of *H. tebenquichense* PA, 2,3-di-O-phytanyl-snglycero-1-phospho-(3'-sn-glycerol-1'-methylphosphate) (PGP-Me), is a ligand for scavenger receptors class A (SRA1) [16] highly expressed on macrophages and dendritic cells. On the other hand, NA consist almost exclusively of bacterioruberin (BR), and its precursors (2-isopentenyl-3,4-dehydrorhodopin (IDR), bis-anhydrobacterioruberin (BABR), and mono-anhydrobacterioruberin (MABR)), together with minute amounts of carotene, lycopene and phytoene [18]. BR is a dipolar C50 carotenoid with four terminals hydroxyl groups responsible for the red colour of the halophilic Archaea [19]. BR acts as cell membrane stabilizer, confers protection against the natural exposition to high UV radiation [20], and displays potent antioxidant activity [21, 22]. Different to the C40 carotenoids identified in bacteria, algae, fungi, and plants, BR has 13 conjugated double bonds and is highly efficient scavenger of RNS, ROS, and quencher of singlet oxygen [23, 24]. Moreover, BR shows higher antioxidant, antihaemolytic and anticancer activities than the well-known β-carotene [23, 25, 26]. However, the high hydrophobicity and susceptibility to chemical degradation due to the 13 conjugated double bonds of the BR, discourages its oral administration.

Our hypothesis is that combination of BR and Dex in macrophage targeted-gastrointestinal resistant nanoparticles could be beneficial for IBD treatment. Hence, here we report the structural features and *in vitro* activity of ultra-small macrophage-targeted nanostructured archaeolipid carriers (NAC) having a core loaded with BR extract and Dex, covered by a PA shell (to confer structural endurance, making the nanoparticle suitable for oral administration and macrophages targeted [27]). The activity of such nanoparticles (NAC-Dex) was assessed on a gut inflammation model, made of Caco-2 cells grown on the apical side and PMA differentiated THP-1 cells grown at the basolateral side of cell culture porous inserts membrane stimulated with lipopolysaccharide (LPS). Histology, immunohistochemistry and transepithelial electrical resistance (TEER) of the gut model as well as release of proinflammatory cytokines IL-8 and TNF-α and intracellular ROS were determined, in the absence and presence of LPS stimuli. Then, the effect of NAC-Dex on the structure of inflamed epithelia and the release of inflammatory cytokines, either before or after submitted to a gastrointestinal digestion process was determined and compared with that of Dex loaded into conventional nanostructured lipid carriers lacking PA and BR extract (NLC-Dex).

2. Materials and methods

2.1 Materials

Compritol ATO 888 (Compritol) was a gift from Daltosur SRL (Gattefosse). Soybean phosphatidylcholine (SPC, purity >90%) was a gift from Lipoid, Ludwigshafen, Germany. Miglyol 840 was a gift from Etilfarma SA, Argentina. Dexamethasone (Dex), 2,2-diphenyl-1-picrylhydrazyl (DPPH), 6-hydroxy-2,5,7,8-tetramethylchroman-2-carboxylic acid) (Trolox), 2,2'-azino-bis(3-ethylbenzothiazoline-6-sulphonic acid) (ABTS),), lipopolysaccharides from Escherichia coli 0111:B4 (LPS), 3-(4,5-dimethylthiazol-2-yl)-2,5-diphenyl tetrazolium bromide (MTT), 2- Mercaptoethanol, Phorbol 12-myristate 13-acetate (PMA), pepsine, bovine serum albumin, Mowiol and 3-(2′-benzothiazolyl)-7-diethylaminocoumarin (coumarin-6, C6) were from Sigma-Aldrich (MO, USA). 2',7'-dichlorodihydrofluorescein diacetate (H_2DCFDA), TO-PRO-3 and rhodamine-conjugated phalloidin was from Thermo Fisher Scientific, the USA. Tween 80 (T80) was acquired from Merck. Porcine pancreatic lipase was a gift from Gador (Biozym). Triton X-100 was from Biopack, Argentina. Roswell Park Memorial Institute 1640 (RPMI), Modified Eagle Medium (MEM), penicillin-streptomycin sulphate, glutamine, sodium pyruvate and trypsin/ethylenediamine tetra acetic acid were from Gibco®, Life Technologies (NY, USA), fetal bovine serum (FBS) was from Internegocios, Cordoba, Argentina. The other reagents were of analytic grade from Anedra, Research AG (Buenos Aires, Argentina).

2.2 Archaebacteria growth, extraction, and characterization of polar archaeolipids (PA) and BR extract

Halorubrum tebenquichense archaeas were grown in 15 l basal medium supplemented with yeast extract and glucose at 40°C and 600 rpm in a home-made bioreactor and harvested after 96 h growth. Total archaeolipids were extracted using the Bligh and Dyer method modified for extreme halophiles [28], and then separated by cold acetone precipitation into an acetone-insoluble fraction (polar archaeolipids, PA) and acetone soluble fraction (BR extract). Both fractions were dried and stored at -20 °C until used.

Between 400 - 700 mg PA and 45 - 90 mg BR extract were isolated from each culture batch. PA was routinely screened by phosphate content [29], and electrospray-ionization mass spectrometry. BR extracts were characterized by UV-visible spectra (300 - 700 nm). BR was quantified measuring the absorbance at 490 nm using an average extinction coefficient ($E_{1cm}^{1\%}$) of 2660 [30]. Thin layer chromatographic (TLC) analysis of BR extract was performed onto a TLC plate (silica gel 60 F254, Merck, Germany) and developed in acetone-petroleum ether (20:80% v/v). Individual spots were scrapped off the TLC, eluted in methanol and UV-visible spectra were recorded. Chromatographic separation of BR extract was performed on a Finnigan HPLC system with photodiode array using C18 Grace Smart RP-18 column (5 μm; 150 x 4.6 mm) set at 25 °C and detection at 490 nm. The following gradient, at a flow rate of 0.8 ml/min, was performed: 0–5 min, 85% methanol; 5–105 min, 100% methanol; 90–105 min, 100% methanol; 105-107 min, 85% methanol; 107-109 min, 85% methanol.

2.3 Preparation and characterization of Dex-nanoparticles (Dex-NP)

Nanostructured lipid carriers (NLC) made of compritol: Miglyol: SPC: T80 (2: 2: 1.2: 3 % w/w) and nanostructured archaeolipid carriers (NAC) made of compritol: BR extract: PA: T80 (2: 2: 1.2: 3% w/w) were prepared by the emulsion-ultrasonication method [31]. Briefly, 60 mg compritol and 60 mg of Miglyol or BR extract (oil phase) were melted at 75-80°C in a water bath. In another separate tube, 36 mg of SPC or TPA and 90 mg of T80 were suspended in 3 ml of ultra-pure water and heated at 75-80°C. The aqueous phase was dispersed for 30 s using an Ultra TurraxT10 Basic (IKA, Germany) and immediately added dropwise into the oil phase at 13,000 rpm at 75-80°C. This hot oil-in-water emulsion was sonicated with a probe-type sonicator (6 mm probe, Sonics& Materials Inc, Vibra Cell Power, USA130 Watt), at 70% amplitude for 10 min. Finally, the nano-emulsion was cooled down at 4°C.

To prepare Dex-NP (NLC-Dex and NAC-Dex), 5 mg Dex were mixed with 120 mg of oil phase and processed as stated before. After solidification, NPs were filtered across a nylon syringe filter membrane of 1.2 μm pore size to eliminate free Dex.

To prepare C-6 labelled NPs (NLC-C6 and NAC-C6), 0.3 mg of C6 (0.1 %w/w) were mixed with 120 mg oil phase and processed as stated before. After solidification, nanoparticles were filtered across a nylon syringe filter membrane of 1.2 μm pore size to eliminate free C6.

2.3.1 Size and ζ potential

Size and ζ potential of NPs were determined by dynamic light scattering (DLS) and phase analysis light scattering (PALS) respectively, using a nanoZsizer equipment (Malvern Instruments, Malvern, United Kingdom). To that aim, NP suspension was 20-fold diluted in distilled water. The refraction index used was 1.33-1.59.

2.3.2 Quantification of dexamethasone

Dex was quantified by spectrophotometry at 243 nm after complete disruption of 20 µl of NP suspension in 3 ml $CHCl_3$:CH_3OH (9:1 v/v). Void NP were used as reference. The absorbance of the sample was compared to a standard curve prepared with Dex in $CHCl_3$:CH_3OH (9:1 v/v).The standard curve was linear in the range 0 - 30 µg/ml with correlation coefficient of 0.99.The encapsulation efficiency (%EE) was calculated using the following relationship: %EE = (amount of drug in the filtrate/amount of drug added) × 100.

2.3.3 Quantification of coumarin-6

Spectrofluorometric quantification of C6 was carried out using λ_{Ex} 465 nm and λ_{Em} 490 nm, after complete disruption of one volume of NPs in 7000 volumes of $CHCl_3$. The fluorescence intensities of the samples were compared to a standard curve prepared with C6 in $CHCl_3$. The standard curve was linear in the range 0.05 - 20 ng/ml with correlation coefficient of 0.991.

2.3.4 Morphology

Morphology of NPs was studied by transmission electron microscopy (TEM) and cryo-electron microscopy (cryo-EM). For TEM, aqueous suspensions of NP were deposited on a carbon grid membrane and the grid covered with a drop of 2% w/v phosphotungstic acid. Then, the grids were air-dried and analysed using a Jeol 1200-EX II (Tokyo, Japan) instrument. For Cryo-EM: samples were prepared in a controlled environment vitrification system (Vitrobot Mark I, FEI, The Netherlands) with controlled temperature (22°C) and humidity (100%). Samples were examined in Jeol JEM-1400Plus (JEOL, Japan) instrument, operating at 120kV. Image collection were made using a CCD camera Gatan Multi Scan 794. Images were not processed after acquisition. Sample preparation and data acquisition were performed at the Electron Microscopy Laboratory (EML)/Brazilian Nanotechnology National Laboratory (LNNano).

2.3.5 Thermal analysis

Calorimetric analysis of physical mixture of lipids and aqueous suspension of NPs were performed using a DSC Q200 TA instrument equipped with a *Refrigerator Cooling System* (RCS90). Briefly, 3-5 mg of lipids or NPs suspension was taken in an aluminium pan. DSC scans were recorded from -50 °C to 90 °C for aqueous suspensions and from -50 °C to 290 °C for bulk material at a heating rate of 10ºC/min, using an empty pan as reference. Melting point and enthalpy were calculated using the software TA Universal analysis provided by TA instruments®. The recrystallization index (R.I.) was calculated according to the following equation: R.I. (%) = ΔH nanoparticles dispersion (J/g)/ [ΔH bulk material (J/g) x concentration lipid phase (%)] x 100

2.3.6 1,1‑Diphenyl‑2‑picrylhydrazyl (DPPH) Radical Scavenging Assay

DPPH radical scavenging assay was performed as described by Jiménez-Escrig et al. (2000) [32] with some modifications. Briefly, 667 µl of 100 µM $DPPH^{*+}$ in methanol was mixed with 83 µl of sample in methanol and incubated for 30 min at 37 °C in the dark on an orbital shaker. Then, absorbance at 580 nm was measured in a Metrolab 330 spectrophotometer, and the radical scavenging capacity (RSA) (%) was calculated as: (Abs negative control -Abs sample)/Abs negative control x 100. Where Abs negative control is the absorbance at 580 nm of sample prepared with 667 µl of $DPPH^{*+}$ plus 83 µl of methanol. Calibration curves of Trolox (1.2-10 µg/ml) and BR extract were done. The inhibitory concentration of the extract providing 50% reduction of the radical scavenging activity (IC50) was calculated from a graph built with log RSA (%) against BR concentration.

The antioxidant activity of NAC was measured after extraction of BR in methanol. Briefly, 250 µl of NPs were mixed with 100 µl of methanol. The mixture was then centrifuged at 9500 g for 10 min, the supernatant was collected and 100 µl of methanol was added to the pellet. After a second centrifugation, the supernatant was mixed with the first one and dried under flux of N_2.

2.4 Stability under gastrointestinal conditions

2.4.1 Colloidal stability in simulated gastric and intestinal fluid

The structural stability, and possible aggregation of NPs into simulated gastric fluid (SGF, 3.2 mg/ml pepsin, 34.2 mM NaCl, pH 1.2) and simulated intestinal fluid (SIF, 150 mM NaCl, 5 mM $CaCl_2$, 5 mM sodium taurocholate, 1.25 mM lecithin, 300 UI/ml porcine pancreatic lipase, 0.5% SDS in Tris-HCl 10 mM pH 6.8) was measured as reported by Higa et al., 2017 [27]. Briefly, 0.1 ml of NPs were diluted with 0.9 ml of SGF and incubated at 37ºC during 30 min. After that, pH was adjusted to 6.8 using 1 M $NaHCO_3$ and then 1 ml of SIF was added and incubated along 2h at 37ºC. Finally, samples were centrifuged for 10 min at 10,000 rpm to remove pancreatic aggregates from the fluid. The particle size and ζ potential after incubation were determined as stated above.

2.4.2 *In vitro* lipolysis

Lipolysis was performed under SIF according to Porter et al, 2001 [33] with minor modifications. Briefly, 300 µl of NPs were added into 3 ml of SIF. The mixture was incubated at 37ºC. The pH was maintained at 6.8 throughout the whole lipolysis process by manual titration with 0.2 M NaOH to neutralize the fatty acid produced by the digestion of lipids. The digestion process was considered complete when the pH change was less than 0.05 units within a 15 minutes interval. Cumulative lipolysis percentage versus time profiles of NPs titrated with NaOH were plotted.

2.5 Cell lines and culture conditions

Caco-2 cells were kindly provided by Dr. Osvaldo Zabal, INTA Castelar, Buenos Aires, Argentina. The human monocyte cell line THP-1 (ATCC® TIB-202™) was supplied by Dr. Paula Barrionuevo, Academia Nacional de Medicina, Argentina.

Caco-2 cells were maintained in MEM with 1% sodium pyruvate, supplemented with 10% FBS, 100 U/ml penicillin 100 µg/ml streptomycin and 2 mM L-glutamine and were grown in a humidified atmosphere of 5% CO_2 at 37°C. THP-1 cells were maintained in complete RMPI medium supplemented with 0.05 mM 2-mercaptoethanol and 1 mM sodium pyruvate. THP-1, monocytes, were differentiated into macrophages by treatment with 162 nM PMA for 24h. Then, the medium was replaced by fresh complete RPMI medium and cells were grown for additional 96 h. The expression of the surface marker CD14 associated with macrophage differentiation was detected by flow cytometry using monoclonal mouse anti-human antibodies IgG1κ CD14-PE (BD Biosciences, San Diego CA, USA).

2.5.1 Cell viability

The viability of cells upon 24 h incubation with void and Dex-NP was measured by the MTT assay. Briefly, differentiated THP-1 and Caco-2 cells were seeded in 96-well plates at a density of 3×10^4 cells per well and grown for 24 h. Then, cells were incubated with series of different concentration of empty NP (20; 200 and 2000 µg/ml of Compritol), and Dex-NP (1.7, 17 and 170 µg Dex /ml - 20, 200 and 2000 µg/ml compritol, respectively). After 24 h of incubation the medium was removed, cells were washed with PBS and 110 µl of 5 mg/ml MTT solution was added to each well. After 3 hours of incubation, the MTT solution was removed, the insoluble formazan crystals were dissolved with 100 µl of dimethyl sulfoxide, and absorbance was measured at 570 nm in a microplate reader (Dynex Technologies, MRX tc, Chantilly, Virginia). The cell viability was expressed as a percentage of the cells grown in medium.

2.5.2 Cellular uptake

The uptake of C6- labelled nanoparticles by macrophages and enterocytes was measured by flow cytometry. Briefly, Caco-2 cells and differentiated THP-1 cells were seeded on 24-wells culture plates at a density of 1.5×10^5 cells per well and grown for 24 h. Then, cells were incubated with 20 µg/ml (compritol) NLC-C6 and NAC-C6 in complete medium for different time periods (1, 3 and 5 h) at 37°C and 4 °C (as a control to determine the unspecific adsorption on cell surface). After incubation, the cells were trypsinized, washed with PBS and a total of 1×10^4 cells were analysed by flow cytometry (BD FACSCalibur™; BD Biosciences, San Jose, CA, USA). Data were analysed using WinMDI 2.9 software (Microsoft, Redmond, WA, USA). The fluorescence was further normalized to the C-6 content of each formulation.

2.6 Gut inflammation model: co-cultured of Caco-2 and PMA differentiated THP-1 cells stimulated with lipopolysaccharides (LPS).

2.6.1 Co-culture development

On one hand, Caco-2 cells were cultured on porous membrane inserts for 20 days to acquired differential and polarized phenotype, functional and morphological like adsorptive enterocytes. Briefly, on day 0 Caco-2 cells were seeded at a density of 1.3×10^5 cells onto ThinCert™ Cell Culture Inserts (12 wells, 0.4 µm pore size PET membrane) and grown for 20 days, the culture medium was changed every other day.

On the other hand, to differentiate THP-1 human monocytes into macrophages, 8×10^5 THP-1 cells per well were seeded on a different 12 well culture plate and induce differentiation with PMA as state before.

On the day 21, the inserts with Caco-2 monolayers were transferred on the plates with differentiated THP-1 cells. Inflammation was induced by 24 h incubation with 10 µg/ml of LPS on the basolateral compartment. Normal co-cultures (non-inflamed) were used as controls.

2.6.2 Monitoring of barrier integrity by TEER

The transepithelial electrical resistance (TEER) of Caco-2 culture and co-culture were measured with an epithelial voltohmmeter (*Millicell-ERS-electrode*, MERSS00001, Millipore Millicell; Billerica, MA, USA). TEER values were normalized subtracting the resistance of empty inserts without cells and multiplying by the insert area and expressed as $\Omega \cdot cm^2$. Monolayers with

TEER value around 350-400 $\Omega \cdot cm^2$ were used for the experiments. TEER of co-cultures were measured 4 and 24 h post inflammation induction.

2.6.3 Anti-inflammatory and antioxidant activity on co-cultures

Anti-inflammatory and antioxidant activity of Dex-NP on inflamed co-cultures were determined by measuring the production of IL-8 and TNF-α in the apical and basolateral compartments, and the ROS production on differentiated THP-1 cells, respectively. Briefly, Dex-nanoparticles at 20 µg/ml Compritol-1.7 µg/ml Dex and free Dex 1.7 µg/ml were applied on the apical compartment and at the same time LPS was added to the basolateral compartment. Upon 24 h of incubation at 37°C, supernatants of apical and basolateral compartments were collected and stored at -20°C for further analysis of cytokines by ELISA as stated above. On the other hand, the generation of ROS was measured on THP-1 cells using the carboxy-H_2DCFDA dye as stated above. Besides, TEER was measured before and 4h and 24 h upon incubation.

Inflamed co-cultures were also incubated with Dex-NP previously submitted to a digestion process. Briefly, 0.1 ml of nanoparticles were incubated with 0.9 ml of SGF at 37ºC for 30 min in an orbital shaker. After that, pH was adjusted to 6.8 using 1 M $NaHCO_3$. Then 1 ml of SIF was added and incubated during 2 h.

2.6.4 TEM

Upon incubation, Caco-2 monolayers were analysed by TEM. Briefly, the monolayer was washed with 2 ml of washing buffer (0.1 M cacodylate - 0.1 M sucrose, pH 7.4) for 15 min and cells were fixed with 2.5% glutaraldehyde for 4 h at 4ºC. Then, monolayers were washed twice with PBS for 15 min and samples were postfixed with 1% OsO_4 in 0.1 M PBS. Cells were dehydrated using a graded ethanol series and acetone and embedded in durcupan resin.

Ultrathin sections of 70 nm, perpendicular to the filter plane, were cut using a Reichert-Jung Ultracut E Ultramicrotome, stained with uranyl acetate, and examined with a Zeiss EM109T transmission electron microscope using an acceleration voltage of 120 kev and images were recorded with a Gatan ES1000W digital camera.

2.6.5 Immunofluorescence staining

Upon incubation, the F-actin cytoskeleton, and nuclei of Caco-2 monolayers were stained with TOPRO3 and rhodamine-labeled phalloidin, respectively. Briefly, monolayers were washed with PBS and fixed overnight with 4% formaldehyde. Then, cells were permeabilized with 0.05 % Triton X-100 in PBS for 10 min, followed by 1h incubation with 3 % bovine serum albumin (BSA) in PBS. Finally, cells were incubated with rhodamine phalloidin (1:1000) and TOPRO3 (1:1000) in 1% BSA in PBS for 1 h at 37 °C. After staining the samples were mounted on slides using mowiol mounting medium. Image acquisition was performed by using a FluoView FV1000 confocal microscope (Olympus, Tokyo, Japan) equipped with a Plapon 60X/1.42 objective.

2.7 Statistical analysis

Statistical analysis was performed by one-way analysis of variance followed by Dunnet's or Tukey test using Prisma 4.0 Software (Graph Pad, San Diego, California). p-value of < 0.05 was considered statistically significant. *$p < 0.05$; **$p < 0.01$; ***$p < 0.001$; ****$p < 0.0001$; n.s. represents not significant ($p > 0.05$).

3. Results

3.1 Characterization of BR extract from *H. tebenquichense*

TLC analysis of BR extract showed 5 spots and the UV-vis spectroscopy revealed the typical three-fingered profile of BR and its derivatives with absorption peaks at 455-460, 490, and 525 nm and two *cis* absorption maxima at 385 and 405 nm (data not shown). HPLC profile showed 16 peaks, each of them displaying the typical three-fingered spectrum of carotenoids (Fig. 1SA). The HPLC peaks with retention times from 64.26 to 85 min could be BR (with maximum absorbance peaks at 461-469, 483-495 and 516-528 nm) (Fig. 1SB, C and D), and different retention times being ones of the different isomers of BR as reported by Naziri et al., 2014 [34]. The HPLC peaks with retention times from 91.84 to 104.95 min were compatible with lycopene (with maximum at 441, 465 and 498 nm, Fig. 1SE) as reported [34].

3.2 Structural features of Dex-NP

NAC were prepared from NLC by replacing Miglyol by BR extract and SPC by PA. Structural features of void and Dex-NP are shown in Table 1. Remarkably, the size of NAC was nearly four folds lower than NLC (~ 66 nm vs ~250 nm). The presence of PA in NAC was responsible for the high negative ζ potential compared to NLC (-32 mV vs -11 mV). Dex did not cause significative changes in size, PDI and ζ potential compared to void NP. When loaded into NLC and NAC, the intrinsic solubility of Dex in aqueous media (71 ± 12 µg/ml) was increased by 18 and 17- folds respectively. The encapsulation efficiency was 76 ± 12% and 72 ± 23 % for NLC-Dex and NAC-Dex, respectively. Compared to solid lipid and archaeolipid nanoparticles previously reported [27],

the presence of Miglyol and BR extract within the NLC and NAC core, respectively increased the Dex content by nearly 1.5-folds. It has been widely described that the less ordered matrix created by the inclusion of liquid lipid into de solid matrix increases the encapsulation efficiency of nanostructured lipid carriers as compared with solid lipid nanoparticles [35]. The broad standard deviation of the Dex content of NAC-Dex could be as consequence of the small size of the core.

TEM images of NAC (Fig. 1SF) and NLC showed irregular shape NPs of roughly 50-60 nm and 100-150 nm mean diameter, respectively. Irregular shape NPs observed by TEM has been also described by other works [36, 37]. It is well known that during observation of soft nanoparticles by conventional TEM, the electron beam might modify the shape or even fuse the particles if the observation is not carried out under low dose conditions, producing artefacts that could be misinterpreted. Because of this, then, we analysed NAC structure by cryo-EM, as it is a very well-known technique for characterization of soft lipid nanoparticles. Cryo-EM images of NAC showed different morphologies that varied with the observation angle, such as ~ 100 nm circles, elongated ellipsoids of low electron density, or ~ 50 nm, needle like shapes of higher electron density (Fig. 1SG). DSC analysis showed a 11.7 and 13.1 °C reduction on the melting point of Compritol for Compritol/Miglyol and Compritol/BR extract mixtures, respectively (Table 1S). A further reduction of 2.5 and 4.4°C on the melting point was observed for NLC, and NAC, respectively. Crystallinity of Compritol was significantly reduced when formulated as NAC but not as NLC, as observed by the lower R.I. for NAC compared with Compritol/BR extract mixtures.

The antioxidant activity of BR extract and NAC was determined using the DPPH radical scavenging assays. The scavenging capacities were linearly dependent on BR concentration, while NLC showed no antioxidant activity. The highest RSA (90 %) was observed at the maximum concentration of BR test (10 µg/ml). BR extract and NAC showed similar antioxidant activity (IC50: 4.8 µg/ml) that was higher than for the standard Trolox (IC50: 7.1 µg/ml). Similar antioxidant activity was reported for BR extracts from *Haloterrigena* sp. (IC50: 4.5 µg/ml for DPPH assay) [24].

3.3. Stability under gastrointestinal conditions

Size retention and lipolytic percentage of Dex-NP incubated in SGF and SIF were determined. SGF and SIF showed a wide peak of 600 nm mean size. Upon incubation, the 250 nm mean size of NLC was observed to be enlarged to a wide peak of 200-900 nm, suggesting aggregation upon interaction with gastrointestinal fluids. NAC in contrast, seemed not to be affected by SGF and SIF since two populations of 50-60 nm and 600 nm, corresponding to NAC and to the gastrointestinal fluids, respectively, were observed (Fig. 1A). Lipolysis of NLC, on the other hand, was almost completed within 30 min (Fig. 1B). In contrast, the lipolysis of NAC was significantly lower than of NLC, reaching an accumulative lipolytic percentage of 25-30% after 60 min.

3.4 Cell viability and uptake

The viability of differentiated THP-1 and Caco-2 cells after 24 h incubation with void and Dex-NP, as determined by MTT, is shown in Fig. 2 A. It was found that the viability of THP-1 and Caco-2 cells did not significantly decrease upon incubation with Dex at all the concentration tested, and void or Dex-NP between 20 and 200 µg/ml of Compritol after 24 h. A higher Compritol concentration (2000 µg/ml) of both Dex-NP led to significant viability loss of 80% for both cell types.

The uptake of C6-labeled NPs by Caco-2 and differentiated THP-1 cells as measured by flow cytometry along 5 h, is shown in Fig. 2 B and C. NAC-C6 but no NLC-C6 were highly uptaken by Caco-2 cells. Both types of NPs were uptaken by differentiated THP-1 cells, but the extent of uptake was higher for NAC than for NLC. At 5 h, NAC-C6 uptake by differentiated THP-1 cells was 2-fold higher than of NLC-C6, while NAC-C6 uptake by Caco-2 cells was 4-fold higher than of NLC-C6.

3.5 Anti-inflammatory and antioxidative activities and morphological changes on Caco-2/THP-1 co-cultures stimulated with LPS

The effect of Dex-NP on a gut inflammation model, consisting of Caco-2 cells and differentiated THP-1 cells stimulated with LPS grown on the apical and basolateral side of cell culture inserts, respectively, was assessed. The model was characterized measuring IL-8 and TNF-α release and intracellular ROS production, besides histology, immunohistochemistry and TEER measurement were performed before and after incubation with non-digested and digested Dex and Dex-NP. The inflamed co-culture released significant amounts of IL-8 in the apical compartment and TNF-α in the basal compartment (Fig. 2SA), produced high amount of ROS (Fig. 2SB) and reduced by ~ 30 % the TEER (Fig. 2SC), compared with the non-inflamed co-culture.

In the non-inflamed co-cultured, the Caco-2 cells formed a polarized monolayer displaying microvilli (M) organized in brush borders and tight junctions in the apical zone (TJ), desmosomes (D) and interdigitations (I) (finger shaped cell membrane folding between cells, characteristic features of epithelial cells) (Fig. 3SA). The F-actin was longitudinally aligned in the cell periphery, forming the characteristic actin belt observed in adjacent epithelial cells (Fig. 4SA). The inflammation caused morphological changes. Although the monolayer was continuous, displaying D and I, the number, extent, and organization of M decreased, and no TJ were observed (Fig. 3A). Actin microfilaments were disorganized, with a significant reduction in intracellular F-actin, as judged by the decreased fluorescence at the level of the peripheral actin belt (Fig. 4SBiii). TNF-α disrupts the assembly of F-actin, which is normally found intercellularly along the edge of the cell. The decreased F-actin is associated with TJ disruption and increased permeability of epithelial barriers [38]. In sum, the typical pathophysiological changes observed in the *in vivo* inflammatory state, such as morphological changes, increased production of pro-inflammatory cytokines and decreased epithelial barrier function were reproduced in the co-culture model. In there, Dex had no effect on cytokine release, but Dex-NP reduced the release of proinflammatory cytokines and reverted the morphological changes induced by LPS. Both NLC-Dex and NAC-Dex showed comparable anti-inflammatory activity, reducing by ~ 65 and 55 % the release of TNF-α and IL-8, respectively (Fig. 4A) but only NAC-Dex decreased by 60 % the induction of ROS (Fig. 4B).

On the other hand, Dex did not increased the TEER (~200 Ω*cm^2) (Fig. 4C) and partly reverted the morphological changes of inflammation: if well the TJ were well defined and showed I, no D were observed, and low amounts of M were detected (Fig. 3SBiii, Table 2S). NLC-Dex, neither increased the TEER (~240 Ω*cm^2) and partly reverted the damages observed in M. Intercellular spaces and F-actin disassembly were observed, resulting in loss of tight assembling, although the D remained present (Fig. 3SBii, 4SBi). On the contrary, NAC-Dex increased the TEER (~300 Ω*cm^2) and reverted the damages in M; as a result, the structural organization resembled that of the non-inflamed model: well defined TJ, I, D (Fig. 3B) and F-actin filaments (Fig. 4SBii).

Finally, after submitting to a simulated gastrointestinal digestion, NLC-Dex completely lost its ability to reduce the release of proinflammatory cytokines. In contrast, NAC-Dex partly retained it, as judged by the 30 % and 70 % reduction in TNF-α and IL-8 release respectively, while it slightly reduced the production of ROS and increased the TEER (Fig. 4 A, B and C).

4. Discussion

BR displays promising beneficial activities at multiple cell levels; nonetheless, its therapeutic use is not popular yet. This is probably because of its physical chemistry lability and hydrophobicity, and because the identification of extremophiles as novel sources of biomaterials has occurred much later than that of green algae and their astaxanthins [25, 39]. The high content of BR and derivatives found in the *H. tebenquichense* acetone soluble fraction used in this work, was in line with the reported abundance of BR and derivatives produced by the *Halorubrum* genus [18, 23, 34]. The structure of labile molecules can be preserved on the other hand, by avoiding oxidation and protecting them from the GI environment if properly formulated as micro- or nano-particles. Surprisingly however, only a single work has reported the preparation of oil-in-water (o/w) micro- and nanoemulsions of BR [40]. Besides, no GI stability or interaction with intestinal cells was assessed. Here the structural features of novel NPs covered with PA, containing BR and Dex in the core, together with their effect on a gut inflammation model, are presented. Due to the presence of PA, NAC-Dex exhibited ultra-small size (66 nm), negative ζ potential (-31.5 mV), were stable under gastrointestinal conditions, and showed high cell uptake by both macrophages (THP-1 cells) and by enterocytes (Caco-2 cells). PA is a mixture of the *sn* 2,3 ether linked phytanyl saturated archaeolipids: phosphatidylglycerophosphate methyl ester (PGP-Me), sulphated diglycosyl diphytanylglycerol diether (SDGD), phosphatidylglycerol (PG) and bisphosphatidyl glycerol (BPG) [16]. As already described by Higa et al., [27], PGP-Me and BPG with two, and PG with one, phosphate groups negatively charged at physiological pH are responsible for the strong negative surface charge, a fact that leads to the lower sized NAC-Dex compared with NLC-Dex. On the other hand, because of their structure, PA are resistant to hydrolysis, oxidation and stereospecific phospholipases [41]; hence PA content was responsible of the higher stability under gastrointestinal conditions of NAC-Dex compared with NLC-Dex. Additionally, as PGP-Me is a ligand of SRA1 mainly express on macrophages, PA presence on NAC-Dex was responsible for their superior uptake by THP-1 cells compared with NLC-Dex. In the case of Caco-2 cells, the smaller size of NAC-Dex could contribute to the higher uptake than NLC-Dex. Zhang et al., [42] and Akbari at el., [43] also reported that smaller size might result in

larger number of nanoparticles interacting with cell membrane area, and consequently higher efficiency of cellular uptake.

The most relevant effects of NAC-Dex, however were observed on a gut inflammation model. *In vitro* models that adequately reproduce both healthy and inflamed intestinal tissue are useful tools for studying mechanisms of intestinal inflammation and new therapeutic drugs. Here, we tested the anti-inflammatory and antioxidant activity of Dex-NP on a co-culture of Caco-2 and PMA-differentiated LPS stimulated THP-1 that mimics the intestine in inflamed state [44, 45]. This model showed typical pathophysiological changes observed in the state of inflammation *in vivo:* release of TNF-α by macrophages, IL-8 by epithelial cells, increased permeability, decreased number and length of epithelial M and reduced number of TJ. We observed that NLC-Dex and NAC-Dex displayed higher anti-inflammatory activity than that of Dex. The higher uptake by THP-1 cells, however, was not correlated with the anti-inflammatory activity of NAC-Dex that was comparable to that of NLC-Dex, probably because NAC-Dex were not optimized for delivering Dex to its cell cytoplasmic receptor, as occurred with Dex-loaded pH-sensitive formulations [16]. However, only NAC-Dex reduced ROS production and produced a reversion on morphological changes induced by inflammation and partial reconstituted the barrier function of the co-culture, that was absent for NLC-Dex and Dex. The barrier function of the intestinal epithelium is maintained partly by TJs between adjacent epithelial cells. TNF-α, produced mainly by activated macrophages, monocytes and T cells, caused TJ disruption both through increased Myosin Light Chain Kinase protein expression and subsequent disassembly of F-actin and decreased ZO-1 expression [38]. Since both NLC-Dex and NAC-Dex reduced TNF-α and IL-8 release, it could be speculated, that the antioxidant activity together with massive internalization of NAC-Dex into Caco-2 cells would help to restore the barrier function. It cannot be discarded hence that the uptake of archaeolipids may finally play a role in the observed barrier repair activity of NAC-Dex.

Concluding, the result suggested that the anti-inflammatory activity was not the only factor needed to restore the function of this experimental epithelial barrier, and that NAC-Dex may be an excellent candidate deserving deeper exploration as intestinal barrier repairing agent.

Credit author statement

LHH performed bacterioruberin extraction and characterization and cytotoxicity, uptake, anti-inflammatory and antioxidant activity. P Schilrreff performed all the co-culture experiments. AMB and HEJ performed preparation and characterized nanoparticles. MAF and RVP performed sample preparation for cryo-transmission electronic microscopies and data interpretation. ELR collaborate with data interpretation and manuscript writing. MJM Project leader, data interpretation and discussion, funding owner.

Declaration of interests

The authors declare that they have no known competing financial interests or personal relationships that could have appeared to influence the work reported in this paper.

Acknowledgements

This work was financially supported by ANPCYT under Grant PICT 2016-4562 and Secretaria de Investigaciones, Universidad Nacional de Quilmes, under Grant Programa de Nanomedicinas-2. HEJ has a fellowship from National Council for Scientific and Technological Research (CONICET). LHH, PS, ELR and MJM, are members of the Research Career Program from CONICET. The authors would like to thank Dr de Farias and Dr Portugal from the EML, LNNano, for sample preparation and data acquisition of Cryo-EM images.

References

[1] Kaplan G.G., The global burden of IBD: From 2015 to 2025. Nat. Rev Gastroenterol Hepatol 2015, 12, 720–727.

[2] Corridoni D., K.O. Arseneau and F. Cominelli, Inflammatory bowel disease. Immunol Lett 2014, 161, 231-235.

[3] Schoultz I. and A.V. Keita, Cellular and molecular therapeutic targets in inflammatory bowel disease-focusing on intestinal barrier function. Cells 2019, 8, 193.

[4] Herulf M., T. Ljung, P.M. Hellstrom, E. Weitzberg and J.O. Lundberg, Increased luminal nitric oxide in inflammatory bowel disease as shown with a novel minimally invasive method. Scand J Gastroenterol 1998, 33, 164–169.

[5] Tian T., Z. Wang and J. Zhang, Pathomechanisms of oxidative stress in inflammatory bowel disease and potential antioxidant therapies. Oxid Med Cell Longev 2017, 4535194.

[6] Guan G. and S. Lan, Implications of antioxidant systems in inflammatory bowel disease. BioMed Res Int 2018, 1290179.

[7] Alzoghaibi M.A., Concepts of oxidative stress and antioxidant defense in Crohn's disease. World J Gastroenterol 2013, 19(39), 6540-6547.

[8] Iborra M., I. Moret, F. Rausell, G. Bastida, M. Aguas, E. Cerrillo, P. Nos and B. Beltrán, Role of oxidative stress and antioxidant enzymes in Crohn's disease. Biochem Soc Trans 2011, 39(4), 1102-6.

[9] Zeng Z., Z. Zhu, Y. Yang, W. Ruan, X. Peng, Y. Su, L. Peng, J. Chen, Q. Yin, C. Zhao, H. Zhou, S. Yuan, Y. Hao, J. Qian, S.C. Ng, M. Chen and P. Hu, Incidence and clinical characteristics of inflammatory bowel disease in a developed region of Guangdong Province, China: a prospective population-based study. J Gastroenterol Hepatol 2013, 28, 1148–1153.

[10] Gómez-Gómez G.J., A. Masedo, C. Yela, M. del P. Martínez-Montiel and B. Casís, Current stage in inflammatory bowel disease: What is next?. World J Gastroenterol 2015, 21(40), 11282-11303

[11] Siegel C.A., Review article: Explaining risks of inflammatory bowel disease therapy to patients. Aliment Pharmacol Ther 2011, 33, 23–32.

[12] Suzuki Y., T. Matsumoto, S. Okamoto and T. Hibi, A lecithinized superoxide dismutase (PC-SOD) improves ulcerative colitis. Colorectal Disease 2008, 10(9), 931–934.

[13] Ng S.C., Y.T. Lam, K.K. Tsoi, F.K. Chan, J.J. Sung and J.C. Wu, Systematic review: the efficacy of herbal therapy in inflammatory bowel disease. Aliment Pharmacol Ther 2013, 38(8), 854-63

[14] Sanchez-Fidalgo S., A Cardeno, M Sanchez-Hidalgo, M. Aparicio-Soto, I. Villegas, M.A. Rosillo and C.A. de la Lastra, Dietary unsaponifiable fraction from extra virgin olive oil supplementation attenuates acute ulcerative colitis in mice. Eur J Pharm Sci 2013, 48(3), 572-581.

[15] Caimi A., F. Parra, M.A. de Farias, R.V. Portugal, A.P. Perez, E.L. Romero and M.J. Morilla, Topical vaccination with super-stable ready to use nanovesicles. Colloids Surf B 2016, 152, 114-123.

[16] Altube M.J, S. Selzer, M.A. de Farias, R.V. Portugal, M.J. Morilla and E.L. Romero. Surviving nebulization-induced stress: dexamethasone in pH-sensitive archaeosomes. Nanomedicine (Lond) 2016, 11(16), 2103-2117

17. Schilrreff P., Y.R. Simioni, H.E. Jerez, A.T. Caimi, M.A. de Farias, R.V. Portugal, E.L. Romero and M.J. Morilla, Superoxide dismutase in nano-archaeosomes for targeted delivery to inflammatory macrophages. Colloids Surf B 2019, 179, 479–487.

18. Calegari-Santos R., R.A. Diogo, J.D. Fontana and T.M. Bonfim, Carotenoid production by halophilic archaea under different culture conditions. Curr Microbiol 2016, 72, 641–651.

19. de Lourdes Moreno M., C. Sánchez-Porro, M.T. García and E. Mellado, Carotenoids' production from halophilic bacteria. Methods Mol Biol 2012, 892, 207–217.

20. Singh O.V. and P. Gabani. Extremophiles: radiation resistance microbial reserves and therapeutic implications. J Appl Microbiol 2011, 110, 851–861.

21. Shahmohammadi H.R., E. Asgarani, H. Terato, T. Saito, Y. Ohyama, K. Gekko, O. Yamamoto and H. Ide, Protective roles of bacterioruberin and intracellular KCl in the resistance of *Halobacterium salinarium* against DNA-damaging agents. J Radiat Res 1998, 39, 251–262.

22. Saito T., Y. Miyabe, H Ide and O. Yamamoto, Hydroxyl radical scavenging ability of bacterioruberin. Radiat Phys Chem 1997, 50, 267–269.

23. Mandelli F., V.S. Miranda, E. Rodrigues and A.Z. Mercadante, Identification of carotenoids with high antioxidant capacity produced by extremophile microorganisms. World J Microbiol Biotechnol 2012, 28, 1781–1790.

24. Squillaci G, R. Parrella, V. Carbone, P. Minasi, F. La Cara and A. Morana, Carotenoids from the extreme halophilic archaeon *Haloterrigena turkmenica*: identification and antioxidant activity. Extremophiles 2017, 21(5), 933-945.

25. Rodrigo-Baños M., I. Garbayo, C. Vílchez, M.J. Bonete and R.M. Martínez-Espinosa, Carotenoids from Haloarchaea and their potential in biotechnology. Mar Drugs 2015, 13, 5508-5532.

26. Hou J. and H.L. Cui, *In vitro* antioxidant, antihemolytic, and anticancer activity of the carotenoids from Halophilic Archaea. Curr Microbiol 2017, 75(3), 266-271.

27. Higa L., H. Jerez, M.A. de Farias, R.V. Portugal, E.L. Romero and M.J. Morilla, Ultra-small, highly negatively charged archaeolipid nanoparticles for active targeting to macrophages of the inflamed mucosa. Nanomedicine (Lond). 2017, 12(10), 1165-1175.

28. Kates M. and SC Kushwaha, In Archaea: A Laboratory Manual, Halophiles Das Sarma and Fleischman, eds. Cold Spring Harbor Laboratory Press, 35–54 (1995)

29. Bötcher C.J.F., C.M. van Gent and C. Pries, A rapid and sensitive submicron phosphorus determination. Anal Chim Acta 1961, 24, 203-4.

30. Britton G., S. Liaaen-Jensen, H. Pfander, A.Z. Mercadante and E.S. Egeland, Carotenoids Handbook. Birkhäuser Verlag, Basel (2004)

31. Silva A.C., E. González-Mira, M.L. García, M.A. Egea, J. Fonseca, R. Silva, D. Santos, E.B. Souto and D. Ferreira, Preparation, characterization and biocompatibility studies on risperidone-loaded solid lipid nanoparticles (SLN): high pressure homogenization versus ultrasound. Colloids Surf B 2011, 86, 158–165.

32. Jiménez-Escrig A., I. Jiménez-Jiménez, C. Sánchez-Mono and F. Saura-Calixto, Evaluation of free radical scavenging of dietary carotenoids by the stable radical 2,2-diphenyl-1-picrylhydrazyl. J Sci Food Agric 2000, 80,1686–1690.

33. Porter C.J. and W.N. Charman, *In vitro* assessment of oral lipid based formulations. Adv Drug Delivery Rev 2001, 50 Suppl 1:S, 127-S147.

34. Naziri D., M. Hamidi, S. Hassanzadeh, V. Tarhriz, B. Maleki Zanjani, H. Nazemyieh, M.A. Hejazi and M.S. Hejazi, Analysis of carotenoid production by *Halorubrum* sp. TBZ126: An extremely halophilic archeon from Urmia Lake. Adv Pharm Bull 2014, 4, 61–67.

35. Joshi M.D., R.H. Müller, Lipid nanoparticles for parenteral delivery of actives. Eur J Pharm Biopharm 2009, 71, 161–172.

36. Kumar R., A. Singh, N. Garg, Acoustic cavitation-assisted formulation of solid lipid nanoparticles using different stabilizers. ACS Omega 2019, 4, 13360−13370.

37. Kumar R., P. Soni, P.F. Siril, Engineering the morphology and particle size of high energetic compounds using drop-by-drop and drop-to-drop solvent−antisolvent interaction methods. ACS Omega 2019, 4, 5424−5433.

38. Ma T.Y., M.A. Boivin, D.M. Ye, A. Pedram and H.M. Said, Mechanism of TNF-alpha modulation of Caco-2 intestinal epithelial tight junction barrier: role of myosin light-chain kinase protein expression. Am J Physiol Gastrointest Liver Physiol 2005, 288, 422–430.

39. Giani M., I. Garbayo, C. Vílchez, R.M. Martínez-Espinosa, Haloarchaeal carotenoids: healthy novel compounds from extreme environments. Mar Drugs 2019, 17, 524.

40. Chaari M., I. Theochari, V. Papadimitriou, A. Xenakis and E. Ammar, Encapsulation of carotenoids extracted from halophilic Archaea in oil-in-water (O/W) micro- and nano-emulsions. Colloids Surf B 2018, 161, 219–227

41. Corcelli A., S. Lobasso, Characterization of lipids of halophilic Archaea, in: A.F. Rainey, A. Oren (Eds.), Methods in Microbiology—Extremophiles, Elsevier, Amsterdam, 2006, pp. 585–613

42. Zhang P., S. Zhao, Y. Yu, H. Wang, Y. Yang, C. Liu, Biocompatibility profile and in vitro cellular uptake of self-assembled alginate nanoparticles. Molecules 2019, *24*(3), 555

43. Akbari A., A. Lavasanifar, J. Wu, Interaction of cruciferin-based nanoparticles with Caco-2 cells and Caco-2/HT29-MTX co-cultures. Acta Biomaterialia 2017, 64, 249-258

38. Al-Ghadban S., S. Kaissi, F.R. Homaidan, H.Y. Naim and M.E. El-Sabban, Crosstalk between intestinal epithelial cells and immune cells in inflammatory bowel disease. Sci Rep 2016, 6, 29783.

39. Kämpfer, A.A., P. Urbán, S. Gioria, N. Kanase, V. Stone, A. Kinsner-Ovaskainen, Development of an *in vitro* co-culture model to mimic the human intestine in healthy and diseased state. Toxicol In Vitro 2017, 45, 31–43.

Figure captions

Fig 1. Stability of nanoparticles in simulated gastrointestinal fluids. (A) Colloidal stability of in simulated gastric (SGF) and intestinal fluids (SIF). (B) Lipolysis percentage versus time profiles of NLC and NAC titrated by NaOH at a constant pH of 6.8. Data is expressed as mean ± SD (n=3).

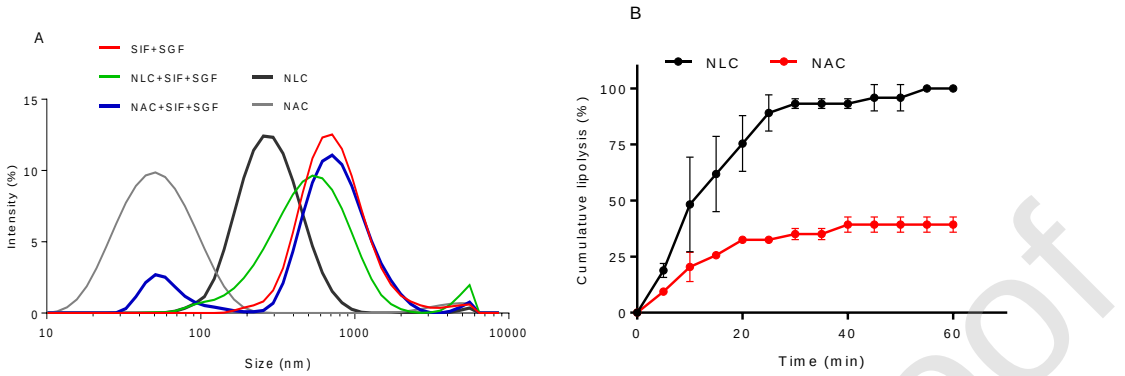

Fig. 2. Cell viability and cellular uptake. (A) Viability upon 24 h incubation with Dex, NLC, NLC-Dex, NAC and NAC-Dex, evaluated by MTT on Caco-2 cells and THP-1 cells (n=3). Kruskal-Wallis multiple comparisons test. Asterisks indicate significant differences between groups and control. (B) Normalized C6 fluorescence intensity of Caco-2 cells and (C) differentiated THP-1 cells after 1, 3 and 5 hours of incubation with C6-labeled nanoparticles. Values are expressed as mean ± SD (n=3).

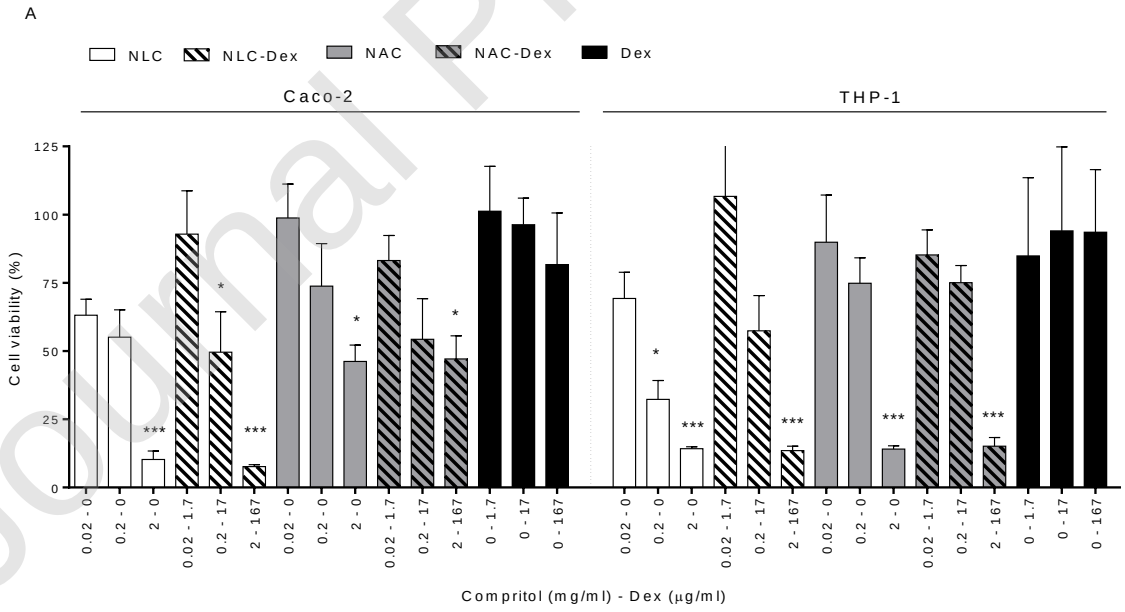

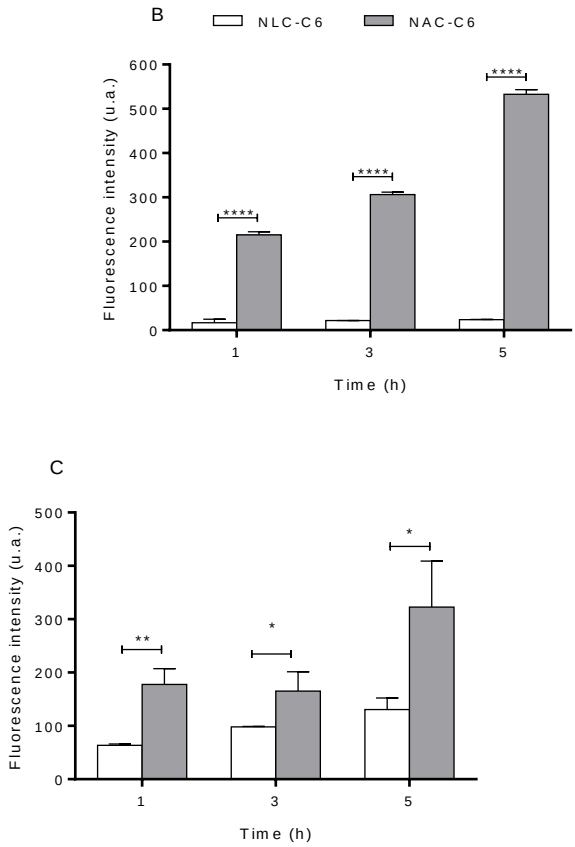

Fig. 3. Ultrathin sections of Caco-2 cells co-cultured with PMA differentiated LPS stimulated THP-1 cells analyzed by transmission electron microscope. (A) Control cells treated with culture medium; (B) cells treated with NAC-Dex. M: microvilli; TJ: tight junctions; D: desmosomes; I: interdigitations.

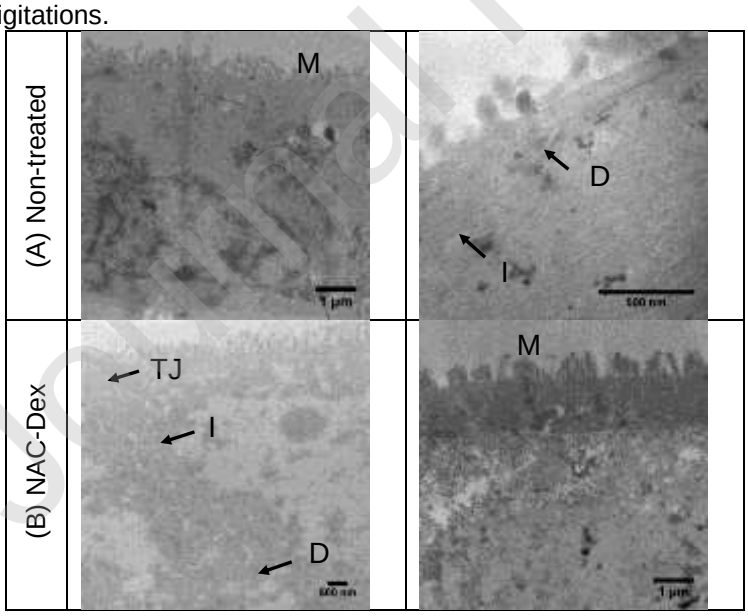

Fig. 4. Anti-inflammatory, antioxidant activity and TEER values on the gut inflammation model upon treatment with Dex and Dex-NP. (A) Pro-inflammatory cytokines release. Each cytokine level was normalized with respect to the level induced by LPS. (B) Fluorescence intensity of carboxy-DCFDA normalized with respect to LPS treated co-cultures. (C) TEER values co-cultures before and 24 h after treatments. Values are expressed by mean value ± S.D (n = 3) and analysed using a one-way ANOVA compared with LPS. Dex and Dex-NP were (+) digested with gastrointestinal fluids or (-) non-digested.

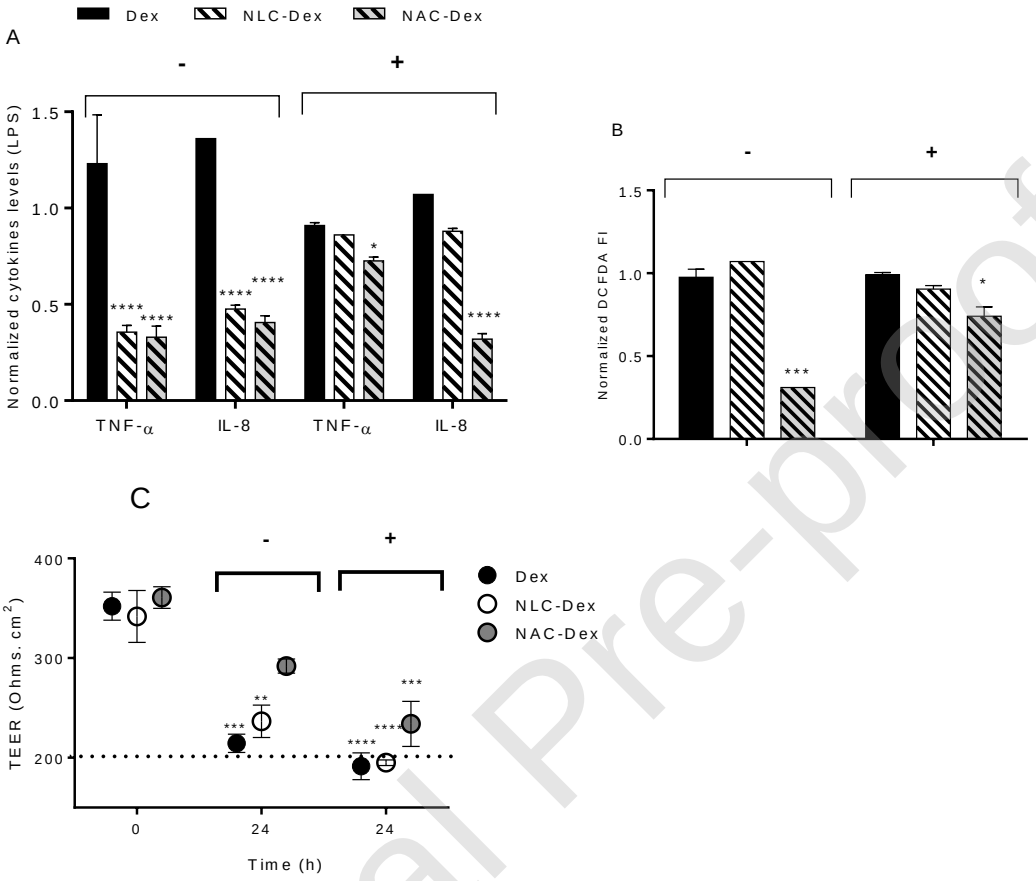

Table 1. Characterization of Dex- and Coumarin 6- loaded nanoparticles.

Formulation	Mean Diameter (nm± SD)	PDI	ζ Potential (mV ± SD)	Dex or C6 (µg/ml ± SD)
NLC	255.5 ± 31.7	0.223 ± 0.067	-13.4 ± 3.7	-
NAC	61.4 ± 9.7	0.355 ± 0.122	-32.5 ± 5.4	-
NLC-Dex	251.1 ± 41.8	0.190 ± 0.041	-13.2 ± 9.8	1269 ± 254
NAC-Dex	66.2 ± 15.0	0.346 ± 0.093	-31.5 ± 5.8	1208 ± 479
NLC-C6	196.5 ± 29.9	0.198 ± 0.062	-18.0 ± 2.1	66 ± 5.5
NAC-C6	52.0 ± 10.8	0.347 ± 0.171	-32.7 ± 6.0	72 ± 0.8

Data are expressed as mean ± standard deviation (SD) from five independent batches.

NLC: ordinary nanostructured lipid carriers; NAC: nanostructured archaeolipid carriers; Dex: dexamethasone; NLC-Dex and NAC-Dex: dexamethasone loaded NLC and NAC, respectively; NLC-C6 and NAC-C6: coumarin 6 loaded NLC and NAC, respectively. SD: Standard Deviation, PDI: Polydispersity Index.